Astronomy Reports, Vol. 46, No. 1, 2002, pp. 49–56. Translated from Astronomicheskiĭ Zhurnal, Vol. 79, No. 1, 2002, pp. 54–62.

Methanol Radio Emission at Millimeter Wavelengths: New Masers at 1.3 and 2.8 Millimeters

V. I. Slysh, S. V. Kalenskiĭ, and I. E. Val'tts

Astro Space Center, Lebedev Institute of Physics, Russian Academy of Sciences, Profsoyuznaya ul. 84/32, Moscow, 117810 Russia

Received October 26, 2000

Abstract—The results of a search for maser emission in the methanol lines 8_{-1}–7_0E at 229.8 GHz, 3_{-2}–$4_{-1}E$ at 230.0 GHz, 0_0–$1_{-1}E$ at 108.9 GHz, and in the $J_1 - J_0E$ series near 165 GHz in star-forming regions are reported. At least two masers and two candidates have been detected at 229.8 GHz. Thus, methanol masers have been detected in the 1-mm band for the first time. At 108.9 GHz, masers have been detected toward G345.01+1.79 and possibly toward M8E as well. Thermal emission was found toward 28 objects. The 229.8-GHz sources are class I masers, whereas the 108.9-GHz sources are class II masers. An analysis using a large velocity-gradient method shows that the 229.8-GHz masers can appear at densities of about 3×10^4 cm^{-3}. The ratios of the flux densities in different class I lines toward DR 21(OH) and DR 21 West can be approximated in models with gas kinetic temperatures of about 50 K. Detection of the 108.9 GHz masers toward G345.01+1.79 and M8E may provide information about the geometry of these objects. © *2002 MAIK "Nauka/Interperiodica"*.

1. INTRODUCTION

The methanol molecule (CH_3OH) is a slightly asymmetric top with hindered internal rotation; it possesses a multitude of allowed transitions at radio wavelengths. The radio emission of interstellar methanol has been actively studied since its discovery by Ball *et al.* [1] in 1970. Narrow, bright, undoubtedly maser lines have been detected at many frequencies, often superimposed on broader thermal features. Currently, methanol masers have been found in hundreds of star-forming regions in our Galaxy and the Large Magellanic Cloud [2]. A classification for methanol masers was first proposed by Batrla *et al.* [3] and later modified by Menten [4]. Menten [4] divides all methanol masers into two classes. Class I includes masers emitting in the lines 7_0–6_1A^+, 4_{-1}–3_0E, 8_0–7_1A^+, etc.; class II includes masers emitting in the lines 2_{-1}–3_0E, 5_1–6_0A^+, 3_1–4_0A^+, etc. A number of theoretical studies devoted to methanol excitation have shown that class I masers are pumped by collisional excitation of rotational levels, and class II masers, by radiative transitions under the action of strong radiation [5, 6]. As a rule, methanol masers simultaneously emit several lines belonging to the same class. It is currently believed that lines belonging to different classes cannot be inverted simultaneously. However, some class I and class II maser sources are associated with the same star-forming regions, and are so closely spaced on the celestial sphere that it is virtually impossible to distinguish between their positions in single-dish observations.

The strongest class I masers have been detected in the 7_0–6_1A^+ transition at 7 mm and the 4_{-1}–3_0E transition at 8 mm. At shorter wavelengths, in the 3-mm and 2-mm bands, weaker masers in the 5_{-1}–4_0E, 6_{-1}–5_0E, and 8_0–7_1A^+ lines have been observed. The situation is similar for class II masers: the strongest masers in the 2_{-1}–3_0E and 5_1–6_0A^+ lines are observed at centimeter wavelengths, and weaker ones are observed in the 3_0–4_1A^+ and J_0–$J_{-1}E$ lines in the 3-mm and 2-mm bands. This wavelength dependence of the line intensity is explained by the decrease in the degree of inversion and optical depth with decreasing wavelength. When deriving the parameters of a maser source, it is useful to know the limiting wavelengths at which maser emission is possible. Therefore, observations of methanol masers at wavelengths shorter than those observed earlier are of interest.

We conducted a search for masers in the 8_{-1}–7_0 line of E-methanol at 229.8 GHz (1 mm). Previously, no searches for methanol masers had been carried out at such high frequencies. According to the theoretical models of Sobolev *et al.* [6], 8_{-1}–7_0E is a class I transition, and 229.8-GHz masers should be observed together with masers in the 7_0–6_1A^+ and 4_{-1}–3_0E transitions, as well as other transitions of this class. In addition to the 229.8-GHz line, the

1063-7729/02/4601-0049$22.00

Table 1. Parameters of the observed methanol lines

Transition	Frequency, MHz	Line strength*	E_u/k, K**
$0_0.1_{-1}E$	108894.20	0.4713	5.23
$1_1{-}1_0E$	165050.19	0.6503	15.48
$2_1{-}2_0E$	165061.14	1.0802	20.13
$3_1{-}3_0E$	165099.31	1.5045	27.10
$4_1{-}4_0E$	165190.53	1.9207	36.40
$5_1{-}5_0E$	165369.44	2.3258	48.01
$8_{-1}{-}7_0E$	229758.76	2.4312	81.27
$3_{-2}.4_{-1}E$	230027.06	0.3543	31.96

Note: *In accordance with Cragg *et al.* [8], **energy is measured relative to the E-methanol ground level $1_{-1}E$.

$0_0{-}1_{-1}E$ line at 108.9 GHz (3 mm), a series of $J_1{-}J_0E$ lines at 165 GHz (2 mm) and the $3_{-2}{-}4_{-1}E$ line (1 mm) were observed. According to statistical equilibrium calculations [6, 7], these lines can be inverted in class II sources.

2. OBSERVATIONS

The observations were carried out on the 30-m radio telescope of the Institut de la Radioastronomie Millimétrique (IRAM) in Pico Veleta (Spain) on August 29–31, 1995. The source list included 36 objects in which strong class I and II masers had been detected earlier in other methanol lines. Table 1 lists the frequencies and strengths of the lines observed. Table 2 presents the antenna parameters: antenna efficiency (AE), main-beam efficiency ($B_{\rm eff}$), forward hemisphere scattering factor ($F_{\rm eff}$), halfpower beamwidth (HPBW), and antenna temperature to flux density conversion factor $S_\nu/T_{\rm A}^*$ at 108, 165, and 229 GHz.

The observations were conducted in an on–off mode with three receivers in all three bands simultaneously. We performed the calibration using a chopper-wheel method. The noise temperatures of the receivers at 1, 2, and 3 mm were $\sim$ 100 K, and the system noise temperature varied in the range 300–1500 K at 3 mm and 1000–3000 K at 1 and 2 mm[1], depending on the weather and source elevation above the horizon. The pointing accuracy was checked using observations of continuum sources, and was no worse than 3″.5. For several sources, we obtained maps with a small number of points (5–10).

We used a 512-channel spectrometer with a resolution of 1 MHz (1.3 km/s) for the observations at 1 mm. The analysis band enabled us to observe the frequencies of the $8_{-1}{-}7_0E$ and $3_{-2}{-}4_{-1}E$ lines simultaneously. The band also included the $19_5{-}20_4A^+$ and $19_5{-}20_4A^-$ methanol lines. To observe the $8_{-1}{-}7_0E$ and $3_{-2}{-}4_{-1}E$ lines with high frequency resolution, the receiver backend was connected in parallel to a 256-channel spectrometer with a resolution of 100 kHz (0.13 km/s), split into two sections of 128 channels each.

We used another 512-channel filter-bank spectrometer with a resolution of 1 MHz (1.8 km/s) for the 2 mm observations. The analysis band enabled us to observe the $J = 1{-}4$ lines of the $J_1{-}J_0$ series simultaneously. A section of an autocorrelator (1000 channels) with a resolution of 80 kHz (0.14 km/s) was connected in parallel to enable observation of the $J = 1{-}3$ lines with high resolution.

In four sources, we observed at the frequency of the $5_1{-}5_0E$ line by retuning the 2-mm receiver to this frequency.

For the 3-mm observations, we used the second section of the autocorrelator, with a resolution of 40 kHz (0.11 km/s).

The data were processed with the CLASS software package. When fitting Gaussians to the $J_1{-}J_0E$ lines, we assumed their LSR velocities and linewidths to be identical.

Table 2. Parameters of the IRAM 30-m radio telescope

Frequency, GHz	AE	$B_{\rm eff}$	$F_{\rm eff}$	HPBW, arcsec	$S_\nu/T_{\rm A}^*$, Jy/K
108	0.57	0.68	0.92	22.0	6.3
165	0.41	0.50	0.90	15.0	8.6
229	0.32	0.39	0.86	10.4	10.5

3. RESULTS

We observed 36 star-forming regions and one galaxy. Emission in at least one methanol line was detected in 30 sources.

In the $8_{-1}{-}7_0E$ transition, we detected narrow maser lines toward DR 21(OH) and DR21 West. These are the first detections of methanol masers at 1 mm. Broad, quasi-thermal lines were detected toward 18 sources. We believe that at least two of these lines represent blends of narrow maser features (see the next section). We detected maser emission in the $0_0{-}1_{-1}E$ line toward G345.01+1.79 and possibly M8E. In addition, we have detected 28 thermal sources in this line; among these was the galaxy IC 342, from which we detected emission at the sensitivity limit. Only thermal lines were found in the $3_{-2}{-}4_{-1}E$ and $J_1{-}J_0E$ transitions. For sources in

[1] Some sources were observed with higher noise temperatures. Such cases are marked in Table 3 by asterisks.

Table 3. Gaussian parameters of the lines

Source	RA (1950) Dec (1950)	Transition	$\int T_A^* dV$, (K km)/s	V_{LSR} km/s	ΔV km/s	T_A^*, K
G345.01+1.79	$16^h53^m19.6^s$	I	5.9(1.0)*	−13.71(0.47)	4.91(0.83)	
	−40°09′46″	II				<0.90
		III	7.2(1.7); 13.7(1.7); 7.8(1.7); 8.7(1.7); 3.3(1.6)*	−13.95(0.32)	6.01(0.00)	
		IV	0.7(0.2)	−22.55(0.11)	1.03(0.25)	
		IV	0.8(0.1)	−21.90(0.01)	0.49(0.04)	
		IV	2.2(0.1)	−13.60(0.09)	4.00(0.22)	
NGC 6334I(N)	$17^h17^m35.4^s$	I	10.4(0.8)*	−4.88(0.20)	5.09(0.47)	
	−35°42′23″	II				<0.6*
		III	7.3(0.9); 8.7(0.9); 9.3(0.9); 7.0(0.8); 8.1(1.4)[3]	−4.27(0.16)	5.34(0.22)	
		IV	11.2(0.2)	−4.64(0.04)	5.42(0.10)	
M8E	$18^h01^m49.7^s$	I				<0.27
	−24°26′56″	II				<0.27
		III				<0.45
		IV	0.4(0.05)	10.66(0.04)	0.83(0.13)	0.45
L379 IRS3	$18^h26^m32.9^s$	I	5.4(0.5)	20.45(0.22)	4.72(1.07)	
	−15°17′20″	II				<0.45
		III	1.9(0.7); 3.2(0.7); 1.9(0.7); 3.1(0.7)	19.78(0.34)	4.56(0.74)	
		IV	3.5(0.2)	19.32(0.13)	5.56(0.43)	
DR 21 West	$20^h37^m07.8^s$	I	1.1(0.2)	−2.55(0.02)	0.34(0.04)	
	42°08′45″	I	2.7(0.3)	−2.16(0.12)	1.70(0.25)	
		II				<0.25
		III				<0.4?
		IV				<0.2
DR 21(OH)	$20^h37^m12.3^s$	I	3.1(0.2)	−1.64(0.14)	4.18(0.28)	
	42°12′11″	I	2.0(0.1)	0.29(0.01)	0.65(0.03)	
		II				<0.2
		III	1.7(0.3); 2.3(0.3); 2.2(0.3); 2.5(0.3)	−2.65(0.20)	5.76(0.31)	
		IV	2.1(0.1)	−2.75(0.08)	4.71(0.17)	

Note: Transition designations: I—$8_{-1}-7_0E$, II—$3_{-2}-4_{-1}E$, III—J_1-J_0E, IV—$0_0-1_{-1}E$. The last column lists 3σ upper limits for the antenna temperature. An asterisk means that the system noise temperature was higher than 3000 K during the observations.

which masers were detected in at least one transition, the line parameters are listed in Table 3 and the spectra are presented in Fig. 1. The results of the observations for other sources are given in a separate paper [18].

4. COMMENTS ON INDIVIDUAL SOURCES

In this section, we briefly describe the emission detected. A more complete description of the maser sources G345.01+1.79 and M8E is given in [9, 10].

G345.01+1.79. In this object, we detected a line at 108.9 GHz that can be decomposed into two components. A narrow line at −22 km/s coincides

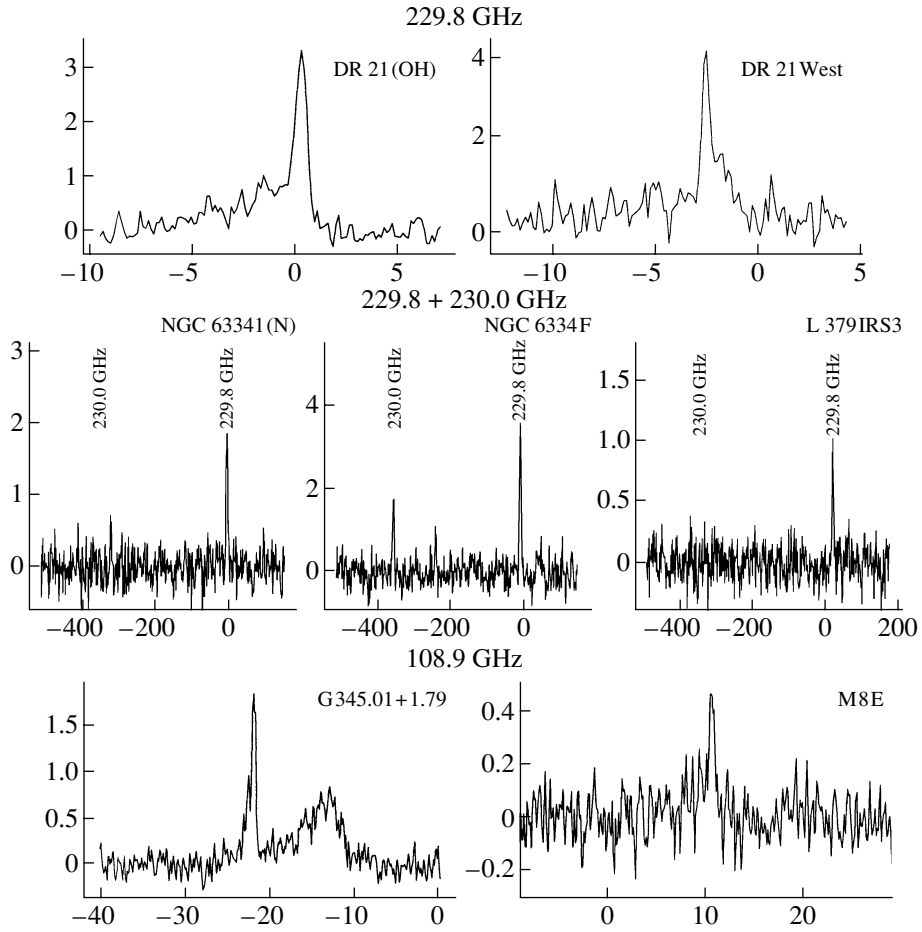

Fig. 1. Spectra of sources in which 229.8-or 108.9-GHz maser emission has been detected; the spectrum of the thermal source NGC 6334F with the 8_{-1}–7_0E (229.8 GHz) and 3_{-2}–$2_{-1}E$ (230.0 GHz) lines is given for comparison. Radial velocities (km s^{-1} relative to the local standard of rest of 8_{-1}–7_0E lines (upper and middle lines) are plotted along the X axis. System temperatures (in Kelvins) are plotted along the Y axis.

in velocity with the masers at 6.7, 12.2, 107.0, and 157 GHz [11, 13, 14] and is undoubtedly a maser line. G345.01+1.79 is currently the only source in which a 108.9-GHz maser has been confidently detected. In addition to the maser line, we detected a broad thermal line at this frequency.

M8E. Emission was detected only at 108.9 GHz. The strongest line was recorded at the point (−10″, 0″) at a projected distance of 12″ to the southeast of the 44.1-GHz maser, which is one of the strongest class I masers. The linewidth is small, 1–2 km/s, depending on the position. This suggests that we are observing either cool, quiescent gas or maser emission at 108.9 GHz. Masers in the 0_0–$1_{-1}E$ line belong to class II [13]. Since none of the strongest class II masers (5_1–6_0A^+ at 6.7 GHz) have been detected in M8E [11], quiescent-gas emission seems more probable. However, we cannot rule out the possibility that, in this source, we are observing a maser pumped by the radiation of an HII region with a relatively low emission measure. This radiation may not be strong enough to populate the 5_1A^+ level. The presence of OH masers [12], which usually accompany class II methanol masers, is consistent with this possibility. A detection of emission in the 2_0–$3_{-1}E$ line at 12.2 GHz would confirm this hypothesis.

L379 IRS3 and NGC 6334I(N). We detected strong, broad lines at 229.8 GHz. Lines found earlier at the same radial velocities in other class I transitions are blends of maser features [15–17]. It is quite probable that the 229.8-GHz lines are also maser lines and consist of narrow features. The nonthermal character of the emission in the 8_{-1}–7_0A^+ line is confirmed by the ratio of its intensity to the intensity in the 3_{-2}–$4_{-1}E$ line at the nearby frequency of 230.0 GHz. In sources with obviously thermal 229.8-GHz emission lines, such as NGC 6334F, Ori KL, G34.26+0.15, W51E1/E2, and W31(1), these intensity ratios are 1.8–3 [18], while, in L379 IRS3 and NGC 6334I(N), the 3_{-2}–$4_{-1}E$ line was not detected

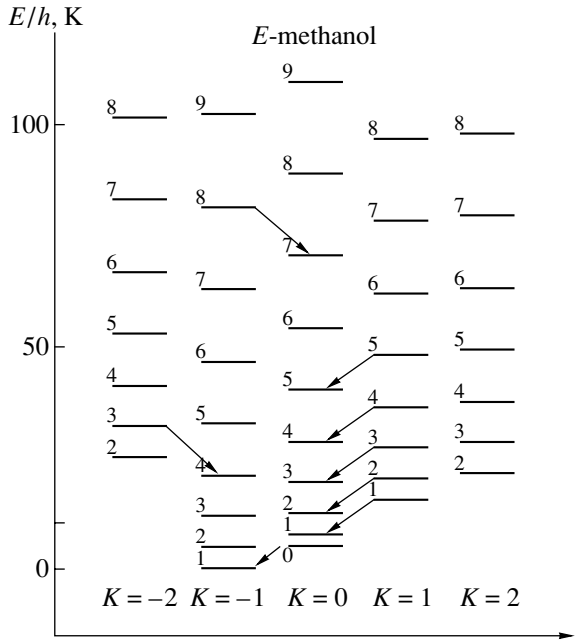

Fig. 2. Energy-level diagram of methanol. The arrows show the transitions detected.

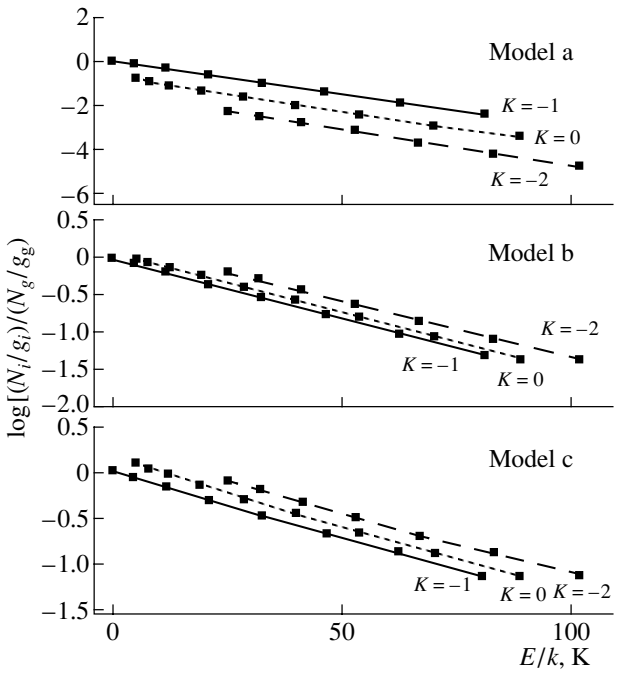

Fig. 3. Ratios of the E-methanol level populations to the population of the ground level $1_{-1}E$, obtained by LVG statistical equilibrium calculations. Points corresponding to the main ladder ($K = -1$) are connected by a solid line; points corresponding to the $K = 0$ and $K = -2$ ladders are connected by the dotted and dashed lines. Models a, b, and c are given in Table 4.

at all, and the corresponding intensity ratio exceeds 2.5 in L379 IRS3 and 3.4 in NGC 6334I(N) (Table 3).

DR 21West. We detected a narrow 229.8 GHz line superimposed on a weaker and broader feature. The narrow line coincides in radial velocity with a strong maser feature in the 7_0–6_1A^+ line at 44.1 GHz [16] and is undoubtedly a maser line. It is interesting that the linewidth at 229.8 GHz is smaller than at 44.1 GHz. This may indicate a saturation of the 7_0–6_1A^+ line, which results in its broadening.

DR 21(OH). We detected a narrow undoubtedly maser line at 229.8 GHz at (0″, 0″), whose radial velocity coincides with that of the strongest maser features in the 7_0–6_1A^+ line at 44.1 GHz [16]. It is possible that the broader feature at (0″, 0″) and the broad asymmetric feature at (10″, 0″) we have detected at 229.8 GHz are blends of the 44.1 GHz maser features.

5. DISCUSSION

5.1. Excitation of Methanol Masers

The upper signal levels of most class I maser transitions lie on the main ladder; i.e., on the sequence of levels with the same quantum number K that contains the ground level. In the case of E-methanol, the ladder of levels with $K = -1$ is the main ladder (Fig. 2). On the contrary, the upper levels of class II maser transitions lie on side ladders. Statistical equilibrium calculations (Fig. 3a) show that, in the case of collisional excitation, the main ladder is overpopulated relative to the adjacent ladders, and transitions with their upper level on the main ladder and lower level on the $K = 0$ side ladder, such as 8_{-1}–7_0E, are inverted.

An external radiation field modifies this pattern. Under the action of radiation, the side-ladder levels are populated more efficiently (Fig. 3, models b, c). As soon as a certain radiation intensity is achieved, the inversion of the class I transitions disappears, but instead the class II transitions are inverted. This is illustrated by the data of Fig. 3 and Table 4, which present the excitation temperatures of four class I and four class II transitions calculated using the large-velocity-gradient (LVG) method for three models. In the absence of external radiation (model a), the class I transitions are inverted. When the radiation temperature exceeds the kinetic temperature of the gas, the inversion of class I transitions disappears, but instead the class II 2_0–$3_{-1}E$ transition is inverted (model b). In this model, the shorter-wavelength 0_0–$1_{-1}E$, 4_1–4_0E, and 3_{-2}–$4_{-1}E$ class II transitions remain noninverted. However, upon further increase of the external radiation intensity (model c), these transitions are also inverted.

Table 4 also demonstrates reductions of the degree of inversion and line optical depth with increasing

Table 4. Results of statistical equilibrium calculations for class I methanol masers and transitions corresponding to class II

Class	Transition	Frequency, GHz	Excitation temperature and optical depth					
			model a		model b		model c	
			T_{ex}, K	τ	T_{ex}, K	τ	T_{ex}, K	τ
I	$4_{-1}-3_0E$	36.169	−1.1	−1.2	9.0	0.8	4.3	0.9
I	$5_{-1}-4_0E$	84.521	−2.8	−0.6	14.0	0.9	8.8	0.9
I	$6_{-1}-5_0E$	132.891	−4.9	−0.2	16.4	0.8	12.6	0.7
I	$8_{-1}-7_0E$	229.759	−10.6	−0.01	19.5	0.4	19.5	0.4
II	4_1-4_0E	165.190	2.5	0.3	48	0.8	−136	−0.2
II	$2_0-3_{-1}E$	12.179	0.4	1.8	−6.0	−0.5	−1.7	−0.9
II	$0_0-1_{-1}E$	108.894	2.8	1.6	60	0.3	−25	−0.4
II	$3_{-2}-4_{-1}E$	230.027	2.4	0.5	157	0.08	−42	−0.2

Note: In model a, the temperature of the external radiation is 2.7 K, the density is 10^5 cm^{-3}, and the specific methanol column density is 10^{-4} cm^{-3} (km/s pc^{-1})$^{-1}$. In model b, these quantities are 50 K, 6×10^{15} cm^2, and 10^{-3} cm^2 (km/s pc^{-1})$^{-1}$. In model c, they are 150 K, 10^{15} cm^2, and 6×10^{-3} cm^{-3} (km/s)$^{-1}$. In all models, the gas kinetic temperature is 25 K. The level population ratios are characterized by rational tempratures of 13, 25, and 26 K in models a, b, and c, respectively.

Table 5. Observed and model flux density in the class I maser lines

Transition	Flux density, Jy					
	DR 21(OH)		DR 21 West		W33 Met	
	model	observations	model	observations	model	observations
$4_{-1}-3_0E$	15.0	13 [20]	50.0	35 [20]	6.0	11 [20]
$5_{-1}-4_0E$	37.8	75[1]	82.0	110 [4]	9.0	18 [21]
$6_{-1}-5_0E$	45.6	67 [15]	82.5	64 [15]	10.7	15 [15]
$8_{-1}-7_0E$	32.7	25	40.0	34	9.7	<5
$9_{-1}-8_{-2}E$	0.003	<0.23 [22]	0.004	<0.25[22]	0.002	0.80 [22]
$7_0-6_1A^+$	35.9	340 [17]	52.5	240 [17]	20.2	70 [17]
$8_0-7_1A^+$	27.2	175[1]	28.5	150 [4]	11.7	13 [23]

Note: The model kinetic temperatures, densities, and specific methanol column density is were DR 21(OH): 60 K, 5.6×10^4 cm^{-3}, 4×10^{16} cm^2 (km/s)$^{-1}$; DR 21 West: 55 K, 3.2×10^4 cm^{-3}, 4×10^{-3} cm^{-3} (km/s)$^{-1}$; W33 Met: 55 K, 5.6×10^4 cm^{-3}, 1.2×10^{17} cm^2 (km/s)$^{-1}$. The observed fluxes without references were obtained in the present work. The gas kinetic temperature was 25 K in all models.

frequency. For instance, in Model a, the optical depth and excitation temperature of the lowest-frequency class I maser considered, $4_{-1}-3_0E$, are −1.2 K and −1.1 K, while those of the highest-frequency maser, $8_{-1}-7_0E$, are −0.01 K and −10.6 K (larger absolute values of the temperature mean smaller degrees of inversion).

5.2. Class I Masers

We have detected narrow maser features in the $8_{-1}-7_0E$ line toward DR 21(OH) and DR 21 West. In other sources, we found only broad quasi-thermal lines. However, at least some of these lines may consist of narrow maser features (see comments for L379 IRS3 and NGC 6334I(N)).

To estimate the conditions under which the masers in the $8_{-1}-7_0E$ line are generated, we analyzed the results of LVG statistical equilibrium calculations. The temperature was varied from 10–100 K[2] in steps

[2]In addition, we performed modeling for a kinetic temperature of 130 K.

Table 6. Modeling of class II maser excitation under the action of emission from a compact HII region ("HII") and hot dust ("dust"). For comparison, observed fluxes for G345.01+1.79 are given

Transition	Frequency, GHz	Observed flux, Jy	Model flux, Jy	
			HII	dust
$5_1-6_0A^+$	6.7	508 [11]	508	508
$2_0-3_{-1}E$	12.2	310 [11]	289	341
$3_1-4_0A^+$	107.0	85.5 [13]	171	166
$0_0-1_{-1}E$	108.9	9.5	89	22
$2_1-3_0A^+$	156.6	21.4 [14]	88	92
$4_0-4_{-1}E$	157.2	54.9 [14]	72	23
4_1-4_0E	165.2	<7	65	<0.01
$3_{-2}-4_{-1}E$	230.0	<9	185	–

Note: The model fluxes were calculated using the data from [6]. Observed fluxes given without references were obtained in the present work. The observed flux for the 4_1-4_0E transition is given at the radial velocity of the maser line (-22.5 km/s).

of 5 K, the density was varied from 10^4-10^8 cm^{-3}, and the specific methanol column density varied in the range $4\times10^{13}-4\times10^{17}$ (km/s)$^{-1}$. We assumed the absence of any external radiation, except for the cosmic microwave background.

The calculations show that masers in the $8_{-1}-7_0E$ line that are comparable in intensity with masers in $4_{-1}-3_0E$, $5_{-1}-4_0E$, and other class I lines can arise at gas temperatures of 50–60 K, typical of Galactic molecular clouds. Table 5 lists the observed flux densities for DR 21(OH), DR 21 West, and W33 Met in various class I lines, as well as the flux densities for models selected as the best fits according to a χ^2 criterion[3]. The calculated models describe the observed line intensity ratios for E-methanol fairly well. The models for the $7_0-6_1A^+$ line underestimate the flux densities compared to the observed values. This may be due to the simplicity of the models, in which we assumed that different lines are emitted in the same region. In reality, the masing region may have multiple components (or multiple layers), and the emission in different lines may form in different layers with different physical conditions.

5.3. Class II Masers

In these observations, we detected class II masers only in the $0_0-1_{-1}E$ line toward G345.01+1.79 and possibly M8E. We found only thermal sources In the $3_{-2}-4_{-1}E$ and J_1-J_0E lines.

As noted above, class II masers are generated under the action of strong external radiation. This can be emission from hot dust or free–free radio emission from ultracompact HII regions. We have modeled the excitation of methanol by radio emission from HII regions. As an example, Table 6 lists the results of LVG modeling of a class II maser source. In this model, the gas density was 3×10^6 cm^{-3}, temperature 50 K, and methanol density divided by the velocity gradient 0.5×10^{-1} cm^{-3}/(km/s pc^{-1}). The source is observed against the background of a compact HII region with an emission measure of 3×10^{12} cm^{-6} pc. The dilution factor for the HII region was taken to be 0.5. For comparison, we list flux densities in maser lines of the class II source G345.01+1.79; the model flux density in the $5_1-6_0A^+$ line was taken to equal the observed value, and the flux densities in other lines were calculated from the ratios of the model brightness temperatures in a way similar to that used when modeling the class I masers. A number of models taking into account emission by hot dust were calculated by Sobolev *et al.* [6]; the results for their model no. 6 are also given in Table 6.

The models for pumping by free–free emission from a compact HII region and by emission from hot dust are both in reasonable agreement with the observational data. The agreement with the flux at 6.7 GHz was predetermined; the predicted fluxes in the lines at 12.2 GHz, 107.0 GHz, 157.2 GHz agree with the observations fairly well. The models overestimate the fluxes for the lines at 108.9 GHz and 156.6 GHz. The largest discrepancy with the observations is shown by the predictions of the HII

[3]The LVG method enables calculation of the line brightness temperature, but does not yield source sizes, so that we could not use it to estimate the flux densities. Therefore, we ascribed the observed value to the model flux density in the $4_{-1}-3_0E$ line and determined the flux densities in the remaining lines from the ratios of the model brightness temperatures, assuming the sizes of each source in all the lines to be identical.

model for the lines at 165.2 and 230.0 GHz: the model predicts large fluxes, which are certainly not observed. At the same time, the dust model predicts an absence of an appreciable flux at these frequencies, in agreement with the observations. Thus, the model for pumping by emission from hot dust describes the observations better. However, the difference between the HII and dust models is purely formal, since real HII regions also contain hot dust mixed with the ionized gas.

Thus, the results of our observations lead us to conclude that modeling of class II methanol masers should take into account pumping by emission from hot dust.

6. CONCLUSIONS

As a result of our 1-mm, 2-mm, and 3-mm observations, we have detected both maser and thermal methanol sources. Methanol masers have been detected at 1 mm for the first time. We found a unique maser in the $0_0-1_{-1}E$ line at 3 mm.

Masers in the $8_{-1}-7_0E$ line that are comparable in intensity with masers in the lines $4_{-1}-3_0E$, $5_{-1}-4_0E$ and other lines belonging to class I can arise at gas temperatures of 50–60 K and densities of $3-6\times10^4$ cm^{-3}, typical of Galactic molecular clouds.

ACKNOWLEDGMENTS

The authors are grateful to Dr. Gabriel Paubert and other colleagues from the Pico Veleta Observatory for help with the observations. This work was partially supported by the Soros Foundation (grant MND300) and the Russian Foundation for Basic Research (project no. 95-02-05826).

REFERENCES

1. J. A. Ball, C. A. Gottlieb, A. E. Lilley, and H. E. Radford, Astrophys. J. Lett. **162**, L203 (1970).
2. A. J. Beasley, S. P. Ellingsen, M. J. Claussen, and E. Wilcots, Astrophys. J. **459**, 600 (1996).
3. W. Batrla, H. E. Matthews, K. M. Menten, and C. M. Walmsley, Nature **326**, 49 (1987).
4. K. M. Menten, in *Proceedings of the 3rd Haystack Observatory Meeting "Skylines,"* Ed. by A. D. Haschick and P. T. P. Ho, Astron. Soc. Pac. Conf. Ser. **16**, 119 (1991).
5. D. M. Cragg, K. P. Johns, P. D. Godfrey, and R. D. Brown, Mon. Not. R. Astron. Soc. **259**, 203 (1992).
6. A. M. Sobolev, D. M. Cragg, and P. D. Godfrey, Mon. Not. R. Astron. Soc. **288**, L39 (1997).
7. M. A. Voronkov, Pis'ma Astron. Zh. **25**, 86 (1999) [Astron. Lett. **25**, 149 (1999)].
8. D. M. Cragg, M. A. Mekhtiev, and R. P. A. Bettens, Mon. Not. R. Astron. Soc. **264**, 769 (1993).
9. I. E. Val'tts, Astron. Zh. **76**, 189 (1999) [Astron. Rep. **43**, 157 (1999)].
10. I. E. Val'tts, Pis'ma Astron. Zh. **24**, 910 (1998) [Astron. Lett. **24**, 788 (1998)].
11. J. L. Caswell, R. A. Vaile, S. P. Ellingsen, and R. P. Norris, Mon. Not. R. Astron. Soc. **274**, 1126 (1995).
12. J. L. Caswell, Mon. Not. R. Astron. Soc. **274**, 215 (1998).
13. I. E. Val'tts, S. P. Ellingsen, V. I. Slysh, *et al.*, Mon. Not. R. Astron. Soc. **310**, 1077 (1999).
14. V. I. Slysh, S. V. Kalenskii, and I. E. Val'tts, Astrophys. J. **442**, 668 (1995).
15. V. I. Slysh, S. V. Kalenskii, I. E. Val'tts, and V. V. Golubev, Astrophys. J. Lett. **478**, L37 (1997).
16. L. R. Kogan and V. I. Slysh, Astrophys. J. **497**, 800 (1998).
17. A. D. Haschick, K. M. Menten, and W. Baan, Astrophys. J. **354**, 556 (1990).
18. V. I. Slysh, S. V. Kalenskiĭ, and I. E. Val'tts (2001) (in press).
19. V. I. Slysh, S. V. Kalenskii, I. E. Val'tts, *et al.*, Astrophys. J., Suppl. Ser. **123**, 515 (1999).
20. S. Liechti and T. L. Wilson, Astron. Astrophys. **314**, 615 (1996).
21. S. V. Kalenskiĭ, V. I. Slysh, I. E. Val'tts, *et al.*, Astron. Zh. **78**, 31 (2001) [Astron. Rep. **45**, 26 (2001)].
22. V. I. Slysh, S. V. Kalenskii, and I. E. Val'tts, Astrophys. J. Lett. **413**, L133 (1993).
23. I. E. Val'tts, A. M. Dzyura, S. V. Kalenskiĭ, *et al.*, Astron. Zh. **72**, 22 (1995) [Astron. Rep. **39**, 18 (1995)].
24. R. L. Plambeck and K. M. Menten, Astrophys. J. **364**, 555 (1990).

Translated by G. Rudnitskiĭ